Microscopic description of surface superconductivity

M. D. Croitoru,[1,*] A. A. Shanenko,[1] Y. Chen,[2] A. Vagov,[3] and J. Albino Aguiar[1]

[1]*Departamento de Física, Universidade Federal de Pernambuco, Av. Prof. Aníbal Fernandes, s/n, 50740-560, Recife-PE, Brazil*

[2]*Department of Physics, Zhejiang Sci-Tech University, 310018 Hangzhou, China*

[3]*Institute of Theoretical Physics III, The University of Bayreuth, 95447 Bayreuth, Germany*

(Received 8 May 2020; revised 24 July 2020; accepted 30 July 2020; published 20 August 2020)

In this work, we revisit the problem of superconductivity under the influence of boundary effects. By solving the Bogoliubov-de Gennes (BdG) equations for the tight-binding model, we demonstrate that the critical temperature of the nucleation of superconductivity near a sample surface can be considerably enhanced as compared to its bulk value. To bring to light this effect, we investigate different methods to solve numerically the BdG equations, including the continuous and Anderson approximations, and perform the calculations for a wide range of the system parameters. We obtain that all the self-consistent BdG eigenstates are delocalized and occupy the entire volume of the sample. Our results reveal that the enhancement of the surface critical temperature originates from the quantum interference of different BdG states contributing to the order parameter. We also find that the surface enhancement is the largest when the conduction band is symmetric with respect to the Fermi level, particularly, the half filling is an important proviso for the pronounced surface effect on the critical temperature. The approximate continuous model as well as the Anderson approximation do not capture the main feature of the surface effect. In addition, our study of this effect versus surface roughness reveals its fragile character.

DOI: 10.1103/PhysRevB.102.054513

I. INTRODUCTION

The boundary effect near the surface of a superconductor, sometimes referred to as *surface superconductivity*, is very important for a manifold of physical phenomena, including, e.g., tunneling, photoemission, critical current, nucleation field H_{c3}, Andreev reflection, etc. The classical work by Saint-James and de Gennes (SJdG) [1–3] predicted that in clean samples the nucleation of superconducting regions in a decreasing magnetic field should always occur near the surface of the sample before the onset of superconductivity in the bulk of the material. Their analysis based on the linearized Ginzburg-Landau (GL) equations demonstrated existence of superconducting sheaths close to a surface of a type II superconductor, placed in a field $H_{c2} \leqslant H \leqslant H_{c3}$ (H_{c2} is the second critical magnetic field).

There has been an exciting string of developments over the past years in studies of surface superconductivity [4–7]. In particular, it was shown that in the case of pure superconductors, the ratio H_{c3}/H_{c2} reveals a noticeable temperature dependence and dependence on the character of reflection at the surface [5,6,8]. Proximity to the surface was also shown to modify the pairing interaction (the so-called twinning-plane superconductivity) [9–11]. Studies have also been concerned effects of crystal and pairing anisotropy of single- and two-gap superconducting materials on temperature and angle dependence of the ratio H_{c3}/H_{c2}[12–17] as well as effects of the sample shape and confinement geometry on the surface critical field [18,19]. Surface induced fluctuation corrections to the thermodynamic characteristics have been identified in addition to the usual bulk contributions [20]. Xie H *et al.* [21] have recently demonstrated a nonmonotonic temperature dependence of the ratio H_{c3}/H_{c2}, that reaches its maximum when the mean-free path in the bulk material is of the same order as the zero-temperature superconducting coherence length. Studies of the quantitative correlation between roughness and surface superconducting critical field showed that roughness plays a vital role in various processes occurring in the proximity of boundaries. For example, Agterberg *et al.* [22] stated that the diffusive boundary almost completely suppresses the third critical magnetic field H_{c3} in the Ginzburg-Landau regime at strong disorder. Gorokhov [16] investigated a two-band superconductor in disordered dominated regime and found that the ratio H_{c3}/H_{c2} is varying with temperature that may take values both larger and smaller than SJdG limit.

Unlike the more familiar effect of boundary on the nucleation field, H_{c3}, the role of surface effects on the critical temperature T_c has been unnoticed and remained hitherto largely unexplored. Initial theoretical analysis of the surface effects on T_c came to a conclusion that in conventional superconductors, where the coherence length ξ_0 is much larger than the Fermi wavelength $\sim k_F^{-1}$, T_c is practically unaffected by the boundaries. A more detailed investigation of the surface effects on the critical temperature, performed within the framework of the self-consistent Bogoliubov-de Gennes (BdG) Bethe-Salpeter equations, demonstrated that within simplified studies of a three-dimensional system with a parabolic band of fermions the surface transition temperature T_{cS} is equal to the bulk one T_{cB}, if the electron-electron interaction is of the standard BCS form and reveals a very slight increase with respect to the bulk value in the case of

*mihail.croitoru@df.ufpe.br; mikhail.croitoru@uni-bayreuth.de

superconductors with small ξ_0 and if one takes into account, in addition, the repulsive part of the interaction [23] It was found that the relative increase of T_{cB}, $\tau_S \equiv (T_{cS} - T_{cB})/T_{cB}$ is higher when T_{cB} itself is high [23]. Furthermore, in the vicinity of the surface the order parameter amplitude shows an enhancement for small ξ_0 [23,24], and exhibits pronounced Friedel-like oscillations [25,26]. A very recent work [27], based on the solution of the tight-binding version of the BdG equations, revealed a non-negligible enhancement of the superconducting critical temperature at the surface with $\tau_S \approx 0.2$. This work brought clarity in some aspects of the increase of the critical temperature at the surface T_{cS}, whilst others still remain unclear. In particular, (i) it is so far not understood to what extent this result depends on the system parameters used in the calculations. (ii) The mechanism of this enhancement and the physics behind it remains to a large extent unclear. (iii) The reason to have such different even opposite outcomes/conclusions (indicated above) while studying similar models for surface superconductivity has not been elucidated so far and, keeping this in mind, and (iv) it is also of importance to clarify how the observed enhancement of T_{cS} is sensitive to the formalism used. In particular, it is not clear why the continuous BdG equations, used in Ref. [23], do not predict any non-negligible surface enhancement while the tight-binding formalism does. Moreover, Ref. [28] argued that the Anderson approximation for the BdG formalism works well for surfaces and the question arises if this statement holds also for the surface superconducting temperature enhancement? Finally, (v) the important question of how the critical temperature T_{cS} of superconductivity nucleation at the surface is sensitive to surface roughness has not been analyzed either.

Motivated by the posed questions, here we investigate the surface superconductivity and its effect on the critical temperature. The goal of the work is achieved by employing the BdG formalism combined with the tight-binding model for a single-band material. We also investigate the Anderson approximation for the tight-binding BdG equations and consider the corresponding continuum BdG model. Notice that in this work we study the surface superconducting effect by considering the electronic degrees of freedom only. The surface induced modification in the phonon degrees of freedom is left beyond the present study.

II. MODEL AND GENERAL SETTINGS

A. General settings

To study surface superconductivity, we consider the simplified case of a one-dimensional chain of sites $j = 1, 2, \ldots, N$ along the x axis, each occupied by one single-orbital atom. The electrons are confined inside the chain by infinite potential barriers situated at the sites 0 and $N + 1$. The latter are empty, indicating that the single-electron wave functions vanish there. The neighboring sites are separated by the distance $a = x_{j+1} - x_j$.

We employ the BdG equations [29,30] that can be generally written as (or in in the form of the eigenproblem in the Nambu space, see Ref. [31])

$$E_\alpha|u_\alpha\rangle = \widehat{H}_e|u_\alpha\rangle + \widehat{\Delta}|v_\alpha\rangle, \tag{1a}$$

$$E_\alpha|v_\alpha\rangle = \widehat{\Delta}^*|u_\alpha\rangle - \widehat{H}_e^*|v_\alpha\rangle, \tag{1b}$$

where $|u_\alpha\rangle$ and $|v_\alpha\rangle$ are the quasiparticle and quasihole ket vectors, E_α stands for the Bogoliubov energy, $\widehat{H}_e$ is the single-electron Hamiltonian, absorbing the chemical potential μ, and $\widehat{\Delta}$ denotes the gap operator. The latter is related to the position-dependent order parameter $\Delta(x)$ as $\langle x|\widehat{\Delta}|x'\rangle = \Delta(x)\delta(x - x')$, where $|x\rangle$ is the eigenket of the position operator and $\delta(x)$ is the Dirac delta function. In this work, the Greek indexes are associated with the energy levels while the spatial positions of the atomic sites are marked by the Latin symbols. As a mean-field approach, the BdG equations should be solved in a self-consistent manner, taking account of the self-consistency relation

$$\Delta(x) = \mathrm{g} \sum_{0<E_\alpha<\hbar\omega_D} \langle x|u_\alpha\rangle\langle v_\alpha|x\rangle(1 - 2f_\alpha), \tag{2}$$

where g is the coupling constant, and $f_\alpha = 1/(e^{\beta E_\alpha} + 1)$ is the Fermi distribution of the bogolons. In what follows, g is uniform all over the system, including the region close to the boundary. To remedy the ultraviolet divergence, the sum in Eq. (2) runs over the BdG states with the positive energies $E_\alpha < \hbar\omega_D$, i.e., we have introduced a cutoff in the energy and ω_D is taken to be a typical frequency, in the case of phonons - the Debye frequency. Our results are not sensitive to the choice of the cutoff. The other variant, based on the selection of the single-electron energies [32,33], leads to minor deviations of about few percents. The physical origin of the electron attraction is left unspecified here.

B. BdG equations within the tight-binding model (t-BdG)

In the tight-binding approach, one uses orthonormal, identical, atomic-like orbitals $|j\rangle$, each centered at the corresponding lattice site j ($j \neq 0, N + 1$) so that we have $\langle x|j\rangle = w(x - ja)$ and $w(x - ja) = w(ja - x)$. As mentioned in the previous subsection, the single-electron wave functions associated with the edges $j = 0$ and $N + 1$ are zero. The single-electron Hamiltonian $\widehat{H}_e$ is approximated as [34,35]

$$\widehat{H}_e = \sum_j (\epsilon_s + U_j - \mu)|j\rangle\langle j| - t\sum_{j\delta}(|j\rangle\langle j + \delta| + |j + \delta\rangle\langle j|), \tag{3}$$

where only $\delta \geqslant 1$ neighboring orbitals are coupled and U_j includes both confinement and disorder contributions. The confining part of the interaction is taken as zero at the sites $1, 2, \ldots, N$ (i.e., inside the specimen) and infinite at the boundaries $U_{j=(0,N+1)} \to \infty$. The first term of Eq. (3) describes an electron that can be trapped around any particular lattice site with the eigenenergy $\epsilon_s + U_j$ when the hopping parameter t goes to zero.

To solve numerically the BdG equations (3), they are converted to a matrix form with a subsequent diagonalization of the relevant matrix constructed from the atomic-like orbitals by using

$$|u_\alpha\rangle = \sum_j u_j^{(\alpha)}|j\rangle, \quad |v_\alpha\rangle = \sum_j v_j^{(\alpha)}|j\rangle. \tag{4}$$

Substituting Eq. (4) into Eq. (1) and projecting the result onto $|j\rangle$, one obtains the tight-binding representation of the BdG equations

$$E_\alpha u_j^{(\alpha)} = \sum_{j'} T_{jj'} u_{j'}^{(\alpha)} + \Delta_j v_j^{(\alpha)}, \tag{5a}$$

$$E_\alpha v_j^{(\alpha)} = \Delta_j^* u_j^{(\alpha)} - \sum_{j'} T_{jj'} v_{j'}^{(\alpha)}, \tag{5b}$$

where we use the matrix elements $T_{jj'} = \langle j|\widehat{H}_e|j'\rangle$ and $\langle j|\widehat{\Delta}|j'\rangle = \Delta_j \delta_{jj'}$, with $\delta_{jj'}$ the Kronecker symbol. The gap operator is diagonal since we are dealing with the s-wave pairing and the self-consistency equation (2) becomes

$$\Delta_j = g \sum_\alpha u_j^{(\alpha)} v_j^{(\alpha)*} (1 - 2f_\alpha), \tag{6}$$

where for the energy index we have $\alpha = 1, 2, \ldots, N$ and the tight-binding coupling g is given by

$$g = \mathrm{g} \int_{-\infty}^{+\infty} dx |w(x)|^4. \tag{7}$$

Due to the infinite barriers at the sites 0 and $N+1$, we have $u_0^{(\alpha)} = u_{N+1}^{(\alpha)} = 0$; $v_0^{(\alpha)} = v_{N+1}^{(\alpha)} = 0$, and therefore $\Delta_0 = \Delta_{N+1} = 0$ .Finally, one should take into account the standard normalization condition [29,30]

$$\sum_\alpha \left(\left| u_j^{(\alpha)} \right|^2 + \left| v_j^{(\alpha)} \right|^2 \right) = 1. \tag{8}$$

C. BdG equations within continuous approach (c-BdG)

To obtain the continuous model for the BdG equations (c-BdG), let us reformulate the tight-binding BdG equations in terms of the eigenstates $|\beta\rangle$ of the single-electron Hamiltonian $\widehat{H}_e$ given by Eq. (3). Using the basis of the atomic-like orbitals, one gets

$$|\beta\rangle = \sum_j \phi_j^{(\beta)} |j\rangle, \tag{9}$$

with $\beta = 1, 2, \ldots, N$. The perfect confinement requires $\phi_0^{(\beta)} = \phi_{N+1}^{(\beta)} = 0$, which results in

$$\phi_j^{(\beta)} = \sqrt{\frac{2}{N+1}} \sin(k_\beta j a), \tag{10}$$

with $k_\beta = \beta\pi/a(N+1)$. Using the basis of the single-particle eigenstates, the particle-like and holelike kets are represented by the series

$$|u_\alpha\rangle = \sum_\beta u_\beta^{(\alpha)} |\beta\rangle, \quad |v_\alpha\rangle = \sum_\beta v_\beta^{(\alpha)} |\beta\rangle. \tag{11}$$

As a result, the BdG equations acquire the form

$$(E_\alpha - \xi_\beta) u_\beta^{(\alpha)} = \sum_{\beta'} \Delta_{\beta\beta'} v_{\beta'}^{(\alpha)}, \tag{12a}$$

$$(E_\alpha + \xi_\beta) v_\beta^{(\alpha)} = \sum_{\beta'} \Delta_{\beta\beta'} u_{\beta'}^{(\alpha)}, \tag{12b}$$

where the single-electron eigenenergies (measured from μ) are given by $\xi_\beta = \epsilon_s - 2t\cos(k_\beta a) - \mu$ and $\Delta_{\beta\beta'} = \langle\beta|\widehat{\Delta}|\beta'\rangle$. Equations (12) are solved together with

$$\Delta_{\beta\beta'} = \sum_{\alpha\beta''\beta'''} g_{\beta\beta',\beta''\beta'''} u_{\beta''}^{(\alpha)} v_{\beta'''}^{(\alpha)*} (1 - 2f_\alpha), \tag{13}$$

which follows from the self-consistency equation (6) with the coupling matrix

$$g_{\beta\beta',\beta''\beta'''} = g \sum_j \phi_j^{(\beta)*} \phi_j^{(\beta')} \phi_j^{(\beta'')} \phi_j^{(\beta''')*}. \tag{14}$$

From Eqs. (12) and (13) one finds the site-dependent order parameter (site-dependent gap function) as

$$\Delta_j = \sum_{\beta\beta'} \phi_j^{(\beta)} \phi_j^{(\beta')*} \Delta_{\beta\beta'}. \tag{15}$$

Now we have everything at our disposal to discuss the continuous limit. This limit is specified by the conditions $a \to 0$ for $Na = \text{const}$. Then, the corresponding single-electron dispersion is given by

$$\xi_\beta \approx \epsilon_s - 2t + tk_\beta^2 - \mu = \xi_{\min} + \frac{\hbar^2 k_\beta^2}{2m} - \mu, \tag{16}$$

with the effective band mass $m = \hbar^2/2t$. For the wave function $\psi_\beta(x) = \langle x|\beta\rangle$, one gets

$$|\psi_\beta(x)|^2 = \frac{2}{a(N+1)} \int_0^{a(N+1)} dx' \sin(k_\beta x') \sin(k_\beta x) \delta(x - x'), \tag{17}$$

where the delta function appears from $|\langle x|j\rangle|^2 \simeq \delta(x - ja)$. Hence, for $0 \leqslant x \leqslant L = (N+1)a$, we arrive at the well-known expression

$$\psi_\beta(x) = \sqrt{\frac{2}{L}} \sin(k_\beta x) \tag{18}$$

and the position-dependent order parameter $\Delta(x)$ reads

$$\Delta(x) = \sum_{\beta\beta'} \psi_\beta(x) \psi_{\beta'}^*(x) \Delta_{\beta\beta'}. \tag{19}$$

Notice that the discrete t-BdG equations have exactly N eigenstates and eigenenergies while the continuous c-BdG equations are specified by an infinite number of eigenfunctions.

D. BdG equations in the Anderson approximation (a-BdG)

Obtaining the solution of the BdG equations in a general case requires considerable computational efforts and is often done using various simplifying assumptions. One of those, that is very useful in practical calculations, is the Anderson approximation (a-BdG). It requires only one diagonalization, namely, diagonalization of the single-particle problem. In this approximation $|u_\alpha\rangle$ and $|v_\alpha\rangle$ are expanded in terms of the basis vectors $\beta\rangle$ as

$$|u_\alpha\rangle = \sum_\beta u_\beta^{(\alpha)} |\beta\rangle, \quad |v_\alpha\rangle = \sum_\beta v_\beta^{(\alpha)} |\beta\rangle, \tag{20}$$

where it is assumed that

$$u_\beta^{(\alpha)} = u^{(\alpha)}\delta_{\alpha\beta}, \quad v_\beta^{(\alpha)} = v^{(\alpha)}\delta_{\alpha\beta}. \tag{21}$$

In this case, one looks for the minimum of the free energy functional in the subspace of $|u_\alpha\rangle$ and $|v_\alpha\rangle$ being proportional to $|\alpha\rangle$, see, e.g., Refs. [36–38]. The Anderson approximation is good enough provided that the pairing of two electrons occupying the different states $|\alpha\rangle$ and $|\beta\rangle$ is minor, i.e., $\Delta_{\alpha\beta} \simeq 0$ ($\alpha \neq \beta$), which is typically the case in the presence of the time reversal symmetry. However, we remark that this approximation is exact only for the spatially-independent order parameter (or in case of strong confinement when the interlevel gap is is sufficiently larger then the superconducting gap).

Substituting Eqs. (20) and (21) into Eqs. (12), one finds

$$E_\alpha = \sqrt{\xi_\alpha^2 + |\Delta_\alpha|^2}, \; u^{(\alpha)}v^{(\alpha)*} = \frac{\Delta_\alpha}{2E_\alpha}, \tag{22}$$

with $\Delta_{\alpha\beta} = \Delta_\alpha\delta_{\alpha\beta}$. The diagonal elements Δ_α are obtained by solving the self-consistency gap equation which reads

$$\Delta_\alpha = \sum_\beta g_{\alpha\beta}\frac{\Delta_\beta}{2E_\beta}(1-2f_\beta), \tag{23}$$

with the interaction matrix element given by (see Appendix)

$$g_{\alpha\beta} = g_{\alpha\alpha,\beta\beta}. \tag{24}$$

The site-dependent order parameter Δ_j is calculated as

$$\Delta_j = \sum_\beta |\phi_j^{(\beta)}|^2 \Delta_\beta. \tag{25}$$

As seen, the a-BdG equations is the semi-analytical approach that considerably simplifies the solution of the formalism. Earlier studies conjectured that this approximation can be used for final samples, also in the vicinity of the boundaries.

In the present work, we investigate the surface superconductivity within the t-, c-, and a-BdG equations, comparing the results for Δ_j. The focus of this comparative study is to clearly display the related physics and search for the parametric domain, where the surface superconductivity can be enhanced.

III. RESULTS

In this section we present the results for the order parameter as a function of the temperature T and the site index j, calculated within t-, a-, and c-BdG equations. At a given μ we solve the BdG equations together with the self-consistency relation by iterations until the convergence is reached, governed by the accuracy 10^{-5} [39]. The physical parameters adopted in our calculations are $\epsilon_s = 2t$, $\hbar\omega_D = 5t$, and $N = 128$ (some of data are also shown for $N = 32$). The coupling constant is within the range $1 \leqslant g \leqslant 3$. Below all energies are given in units of the hopping integral t. For the Boltzmann constant we set $k_B = 1$ so that the temperature is also measured in units of t. In addition, throughout this article the chemical potential μ is specified by the corresponding values of the normal state n_e. We note that our conclusions are not sensitive to the present choice of the physical parameters. The same qualitative results are obtained for other values of the coupling g, the cut-of energy $\hbar\omega_D$, and the number of the inner sites N.

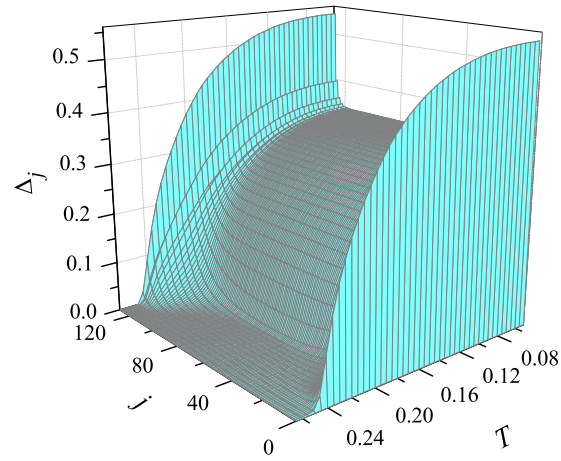

FIG. 1. The order parameter, Δ_j as a function of j and T. The results are calculated within the t-BdG for the half-feeling case $n_e = 1$ with the coupling $g = 2$, the cutoff energy $\hbar\omega_D = 5$, and $N = 128$.

A. Order parameter profile and surface superconductivity in t-BdG

Figure 1 displays the order parameter versus the site number j, for the temperatures ranging from 0 to 0.25. The results are obtained with t-BdG equations for $g = 2$ and for the half-filling case $n_e = 1$. What immediately catches ones, is the behavior of Δ_j near the edges (surface). Namely, the order parameter actually peaks near the boundaries, with several Friedel-like oscillations ensuing towards the center of the sample. Such oscillations of the superconducting condensate are not surprising and have been already reported many times [24–26,28,32,33]. Another remarkable feature in the behavior of the order parameter near the edges is that the condensate here nucleates at temperatures higher than the bulk transition temperature $T_{cB} = 0.206$, associated with the middle of the chain. The survival of superconductivity above T_{cB} is observed in the near-boundary domain of about 20 sites, i.e. its size is much larger than the interatomic distance and close to the coherence length.

In order to consider details of the order-parameter dependence on j near the boundaries, Fig. 2 demonstrates Δ_j for the region $0 < j < 24$. In particular, the condensate profile given in Fig. 2(a) is calculated for the same parameters as that in Fig. 1. One sees that at low temperature $T = 0.05$ the condensate reaches its bulk value already at $j \gtrsim 8$. However, when the temperature increases, the relaxation towards the bulk value Δ_B becomes much slower. When T reaches T_{cB} the gap becomes zero inside the chain ($\Delta_j \to 0$ at $j \gg 1$). However, close to the edges the superconducting condensate still survives for $T > T_{cB}$ up to $T = 0.25$, which determines the upper or the surface critical temperature T_{cS}.

Calculations for the lower electron densities, shown in Figs. 2(b) and 2(c), reveal two tendencies. The first one is that Δ_B and T_{cB} increase at smaller n_e. This is the known feature related to the dependence of the 1D single-particle density of states (DOS) on the position of the chemical potential: it increases when the chemical potential approaches the band edge. The other tendency is surprising. This is the reduction of the surface critical temperature T_{cS} [cf Figs. 2(a)–2(c)]. For

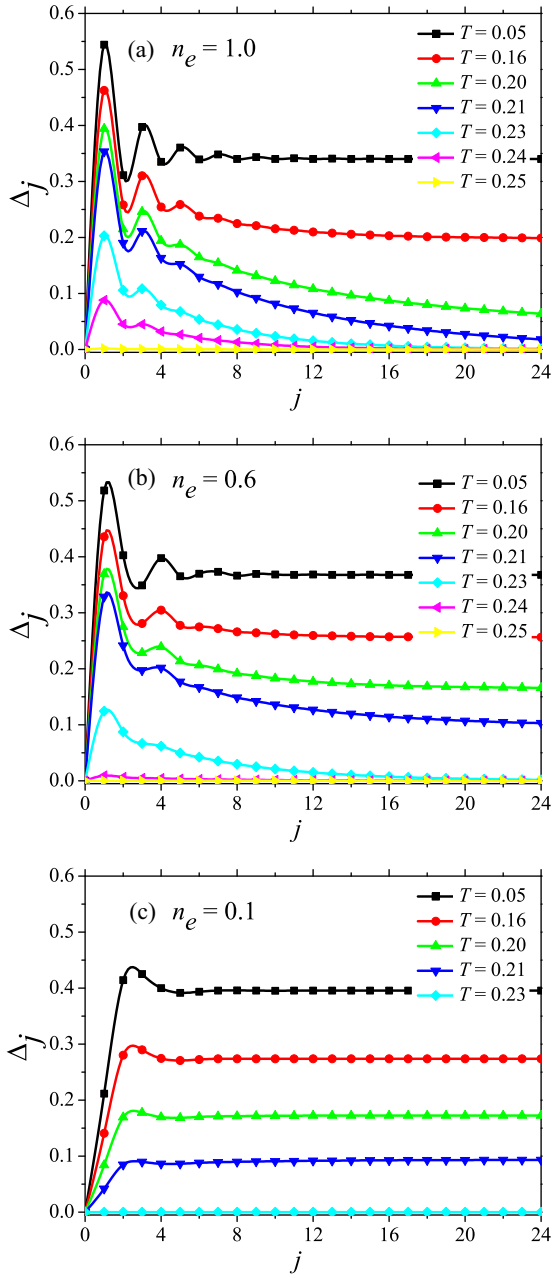

FIG. 2. The gap function Δ_j versus j, as calculated within t-BdG for the electron densities $n_e = 1$(a), 0.6 (b), and 0.1 (c) at different temperatures. Other microscopic parameters are the same as in Fig. 1.

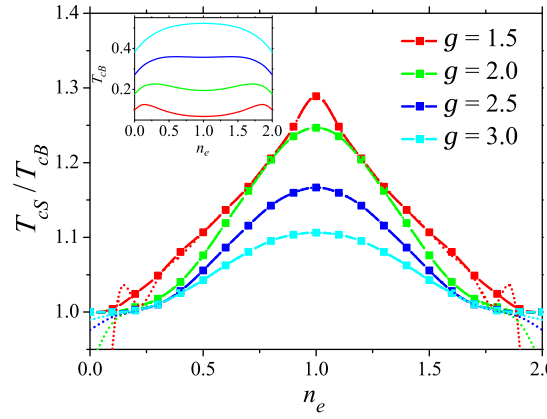

FIG. 3. The ratio T_{cS}/T_{cB} calculated within the t-BdG as a function of n_e for the different coupling constants g. The cutoff energy is $\hbar\omega_D = 5$.

example, in Fig. 2(c), one can see that the site-dependent gap function vanishes in the entire sample at $T > 0.23$. However, for $n_e = 1$ the surface superconductivity is present up to $T_{cS} = 0.25$ for $n_e = 1$, see Fig. 2(a). Respectively, for small densities $n_e \ll 1$ the spatial dependence of the order parameter does not exhibit a long-scale relaxation to Δ_B after the Friedel-like oscillations cease [cf Fig. 2(c)]. One can also notice that the period of the Friedel-like oscillations increases in agreement with decreasing the Fermi wavelength.

The results demonstrate that within the adopted model, a superconductor indeed develops surface superconductivity. The highest enhancement of the surface phenomena occurs when the chemical potential μ is in the proximity to the center of the band. The respective increase of T_{cS} as compared to T_{cB} is illustrated by Fig. 3, which plots T_{cS}/T_{cB} as a function of the electron density n_e. Inset shows, for reference, the respective plot of the bulk critical temperature T_{cB} as a function of the electron density n_e. The calculations are performed for four different values of coupling constant $g = 1.5$, 2.0, 2.5, and 3.0. The results demonstrate that T_{cS}/T_{cB} reaches its maximum in the proximity of $n_e = 1$, while decreases when the chemical potential is near the band edges. One notes that the dependence is symmetric with respect to $n_e \to 2 - n_e$ due to the related symmetry of the single-particle dispersion in the band. The maximal value of T_{cS}/T_{cB} depends on the model parameters. For example, for $g = 3$, it is $T_{cS}/T_{cB} = 1.1$ while at $g = 1.5$ (and the same cut-off energy) it reaches a larger value of almost 1.3. One sees that the decrease in the coupling g pushes the maximum of T_{cS}/T_{cB} up. It is of importance to note that T_{cS}/T_{cB} given in Fig. 3 as a solid line is calculated with T_{cS} selected for the site at which the maximum of Δ_j develops in the proximity of the boundary. In this case the ratio T_{cS}/T_{cB} tends to 1 when $n_e \to 0$ or $n_e \to 2$. If one selects a different site for T_{cS}, say, in the nearest vicinity of the boundary, i.e., for $j = 1$, the ratio T_{cS}/T_{cB} tends to values smaller than 1 when $n_e \to 0$ or $n_e \to 2$ (dotted lines).

B. Surface superconductivity and BdG eigenstates

The results of the calculations presented hitherto show that surface effects give rise to a considerable enhancement of the critical temperature. As discussed the largest enhancement has been observed for the chemical potential approaching the middle of the band. To gain an understanding of the observed behavior, in this subsection we examine the eigenstates of the BdG equations and their contribution to the order parameter.

Figure 4 exhibits the quasiparticle amplitudes $u_j^{(\alpha)}$ (first column), the quasihole amplitudes $v_j^{(\alpha)}$ (second column), and their partial contribution $\Delta_j^{(\alpha)} = u_j^{(\alpha)} v_j^{(\alpha)*}(1 - 2f_\alpha)$ to the order parameter Δ_j (third column) at zero temperature for $\alpha = 1$, 2, 127, and 128. The system parameters are chosen the same as in Fig. 1, where, recall, $n_e = 1.0$. The

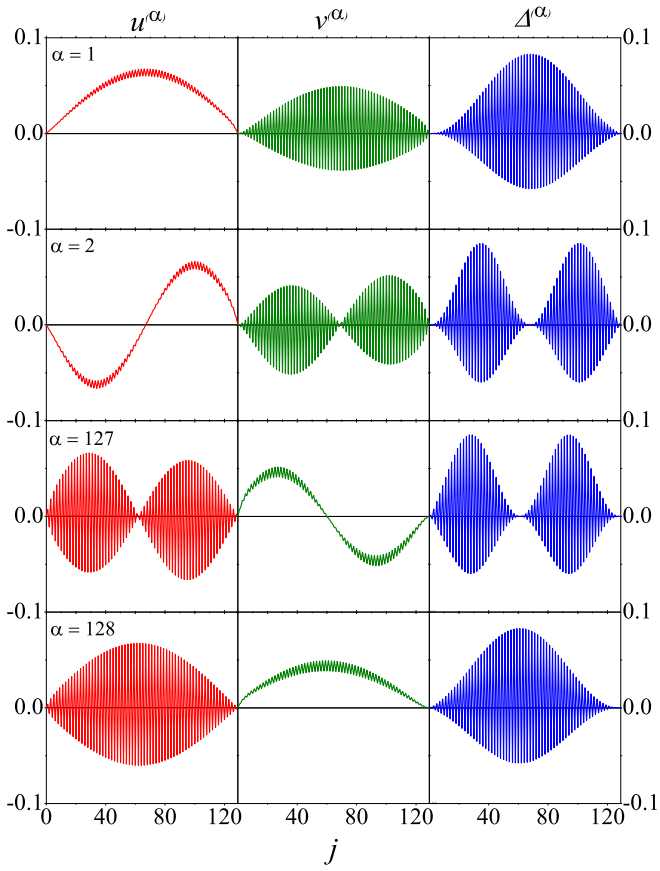

FIG. 4. Typical quasiparticle amplitudes $u_j^{(\alpha)}$ (first column), quasihole amplitudes $v_j^{(\alpha)}$ (second column), and the partial order parameter $\Delta_j^{(\alpha)} = u_j^{(\alpha)} v_j^{(\alpha)*}(1-2f_\alpha)$ (third column) vs j. The rows are for $\alpha = 1,\ 2,\ 127$, and 128 (from above to below). Obtained within t-BdG at the zero temperature for the half-filling case $n_e = 1$. The other model parameters are the same as in Fig. 1.

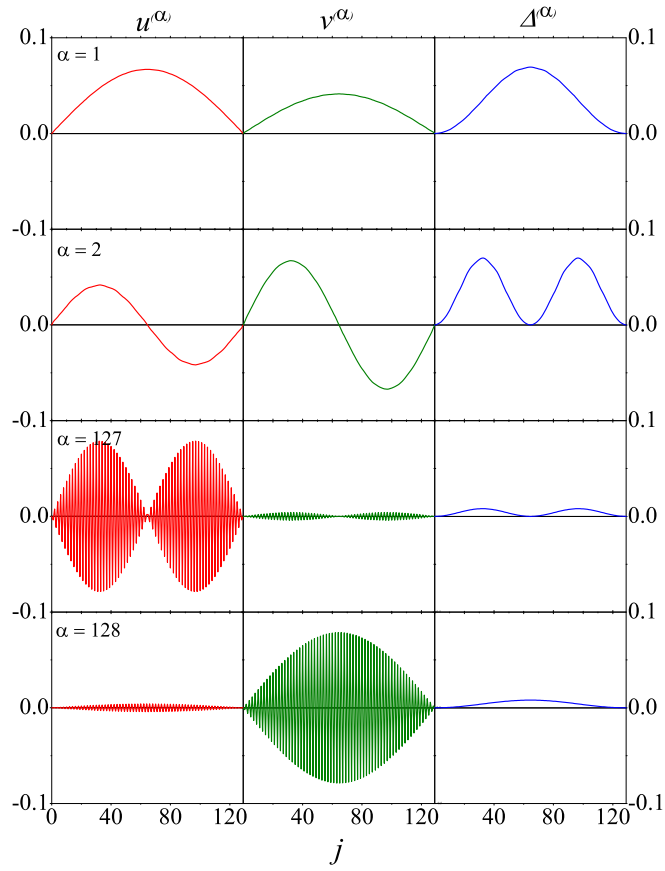

FIG. 5. The same as in Fig. 4 but for the occupation $n_e = 0.1$.

quasiparticle and quasihole wave functions are the standing waves because the quantum confinement restricts the carrier motion. As $\alpha - 1$ is set as the number of nodes of $u_j^{(\alpha)}$ inside the sample, for $u_j^{(1)}$ one can see the typical ground state wave function with zero nodes outside edges. In turn, for $u_j^{(2)}$, we observe one node, and for $u_j^{(N-1)}$ and $u_j^{(N)}$ (with $N = 128$), we have $N-1$ and N nodes, respectively. Moreover, we find that $u_j^{(\alpha)} \approx (-1)^j u_j^{(N+1-\alpha)}$, which is similar to the relation for the single-electron wave functions $\phi_j^{(\alpha)} = (-1)^j \phi_j^{(N+1-\alpha)}$.

The properties of the corresponding quasihole amplitudes are obtained approximately by simultaneously replacing $v \to u$ and $(\alpha = 1) \to (\alpha = N)$. In particular, for $v_j^{(\alpha)}$ one observes $N+1-\alpha$ nodes while there is only $\alpha - 1$ nodes for $v_j^{(N+1-\alpha)}$ and, generally, $v_j^{(N+1-\alpha)} \approx (-1)^j v_j^{(\alpha)}$. As a result, we obtain $u_j^{(\alpha)} v_j^{(\alpha)*} \approx u_j^{(N+1-\alpha)} v_j^{(N+1-\alpha)*}$ and, thus, $\Delta_j^{(\alpha)} \approx \Delta_j^{(N+1-\alpha)}$ (we have $1 - 2f_\alpha = 1$).

Now let us compare the results obtained in the case of the half-filled band with those for low-filling occupations. Figure 5 displays Bogoliubov quasiparticle amplitude $u_j^{(\alpha)}$, quasihole amplitude $v_j^{(\alpha)}$, and the corresponding partial order parameter $\Delta_j^{(\alpha)}$ (the temperature is again zero) for the same values of α but in the case of $n_e = 0.1$. The data are arranged in the same manner as those in Fig. 4. One can see that contrary to the previous half-filling case, now $\Delta_j^{(\alpha)} \neq \Delta_j^{(N+1-\alpha)}$. The reason for this difference is that $u_j^{(\alpha)} \neq (-1)^j u_j^{(N+1-\alpha)}$ and $v_j^{(\alpha)} \neq (-1)^j v_j^{(N+1-\alpha)}$. Based on these results, one can expect that the constructive interference of the partial contributions to Δ_j is less pronounced for $n_e = 0.1$.

This difference between the variants with $n_e = 1$ and $n_e = 0.1$ is related to the degeneracy of the excitation spectrum $E_\alpha = E_{N+1-\alpha}$ for the half-filling case. It is illustrated in Fig. 6, which plots the energy momentum dispersion with the quasimomentum defined as $k_\alpha = \alpha\pi/a(N+1)$. At $n_e = 1$ the dispersion curve has a minimum at $k_\alpha a = \pi/2$ and is symmetric with respect to the transformation $k_\alpha \to \pi/a - k_\alpha$. For the values $n_e = 0.1$ and 0.6, the degeneracy is lifted. The role of the absence of the degeneracy is enhanced at nonzero temperatures due to the appearance of the factors $1 - 2f_\alpha$ in the partial order parameter (this factor is equal to 1 at the zero temperature).

To visualize the contribution of different BdG states to the order parameter, we introduce and calculate the cumulative gap function defined as

$$\Delta_j^{(E)} = \sum_{0<E_\alpha<E} u_j^{(\alpha)} v_j^{(\alpha)*}(1-2f_\alpha), \tag{26}$$

which obviously becomes the true gap function when $E = \hbar\omega_D$. Figure 7 plots $\Delta_j^{(E)}$ as a function of j for different

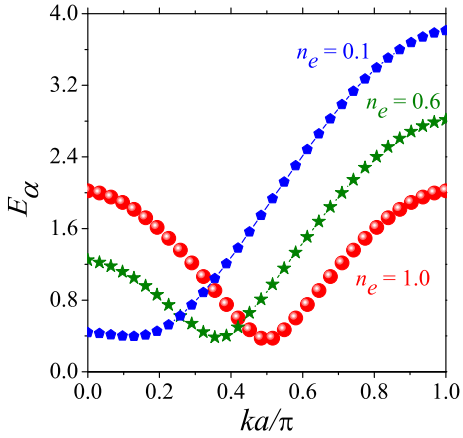

FIG. 6. The excitation energies E_α versus the quasimomentum $k_\alpha > 0$ calculated for $n_e = 0.1$, $n_e = 0.6$, $n_e = 1$. The calculations are done within t-BdG for $N = 32$.

ascending values of E, namely, the lowest curve includes only the lowest energy BdG state, then two lowest BdG states are incorporated and so on. The results for $n_e = 1$ are given in Figs. 7(a) and 7(c) and the case of $n_e = 0.1$ is illustrated in Figs. 7(b) and 7(d). One can see that the surface enhancement of superconductivity at $n_e = 1.0$ is clearly the effect of the constructive interference of different contributing BdG states. At zero temperature this interference results in pronounced peaks of the Friedel-like oscillations. At higher temperatures it gives rise to the appearance of the surface superconductivity that survives even when the order parameter is already suppressed in the middle of the sample [Fig. 7(c)].

At $n_e = 0.1$, the constructive effect of the interference is much less pronounced, in agreement with our conclusion in the previous paragraphs. It still manifests itself in the appearance of the "coherence" peak of the gap function at the edge [Fig. 7(b)] and also in the Friedel-like oscillations. When T increases, this peak in the site-dependent order parameter is still present but it goes even below the bulk value Δ_B [Fig. 7(d)]. As a results, there is no surface enhancement of superconductivity for $n_e = 0.1$. This conclusion is not sensitive to particular values of the coupling, the energy cutoff, and the number of the sites.

To further illustrate the interference effect between different partial contributions $\Delta_j^{(\alpha)}$ to the order parameter it is instructive to perform their spectral decomposition. Figure 8 (a) shows the amplitude spectra of $\Delta_j^{(\alpha)}$ as a contour plot in the $f - \alpha$ plane, calculated for $n_e = 1$. $|\Delta_f^{(\alpha)}|$ ($\Delta_f^{(\alpha)} = FT[\Delta_j^{(\alpha)}]$) is illustrated for all discrete frequency values $f = n/N$ ($n = 0, \pm 1, \pm 2, \dots$) in the range $-f_c$ to f_c with $f_c = 1/2$ (the Nyquist critical frequency). One can clearly observe that all partial contributions to the order parameter oscillate with four dominant frequencies (here we mention only positive values of f, there are their negative counterparts with the same absolute values). The first one is the zero-frequency peak, $f_1(\alpha) = 0$, which equals to the total area under the graph of the partial order parameter, is not important for our further analysis. The second one, with the peak position determined by $f_2(\alpha) = \frac{2f_c}{N}\alpha\theta(\frac{N}{2} - \alpha) + [f_c - \frac{f_c}{N}(2\alpha - N)]\theta(\alpha - \frac{N}{2})$,

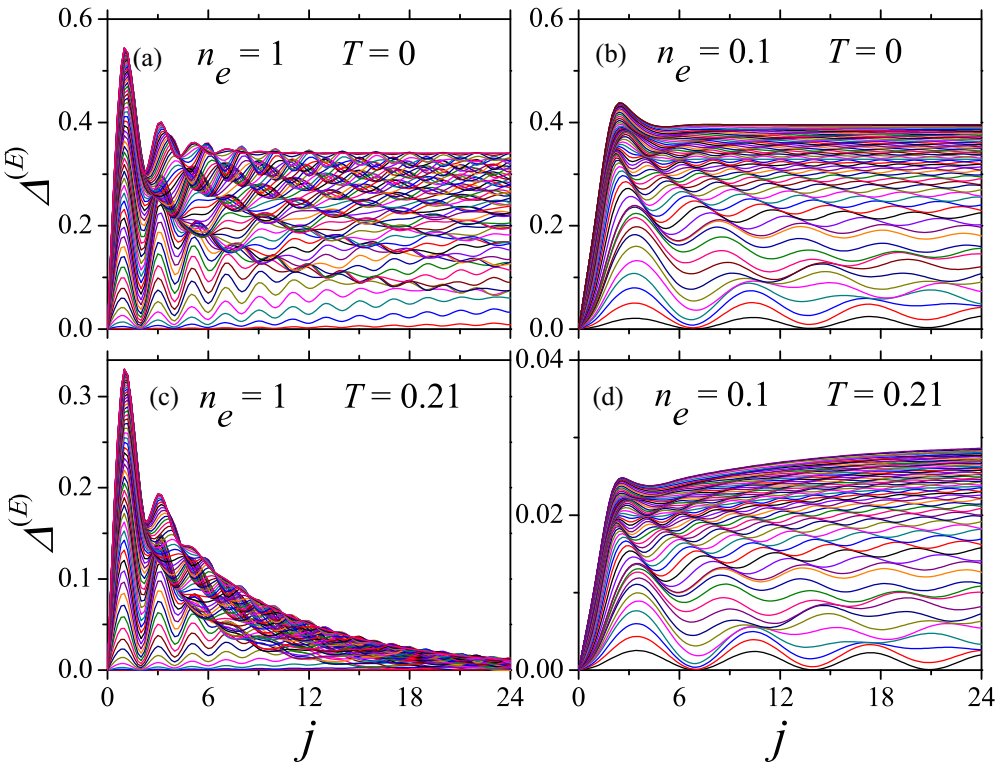

FIG. 7. The cumulative order parameter $\Delta_j^{(E)}$ versus j for different ascending values of $0 < E < \hbar\omega_D$. Calculated within t-BdG for $n_e = 1$ at $T = 0$ (a) and 1.05 (c), and for $n_e = 0.1$ at $T = 0$ (b) and 1.05 (d). The other microscopic parameters are the same as in Fig. 1. The evolution of $\Delta_j^{(E)}$ with increasing E allows one to trace the constructive interference of the contributing BdG states.

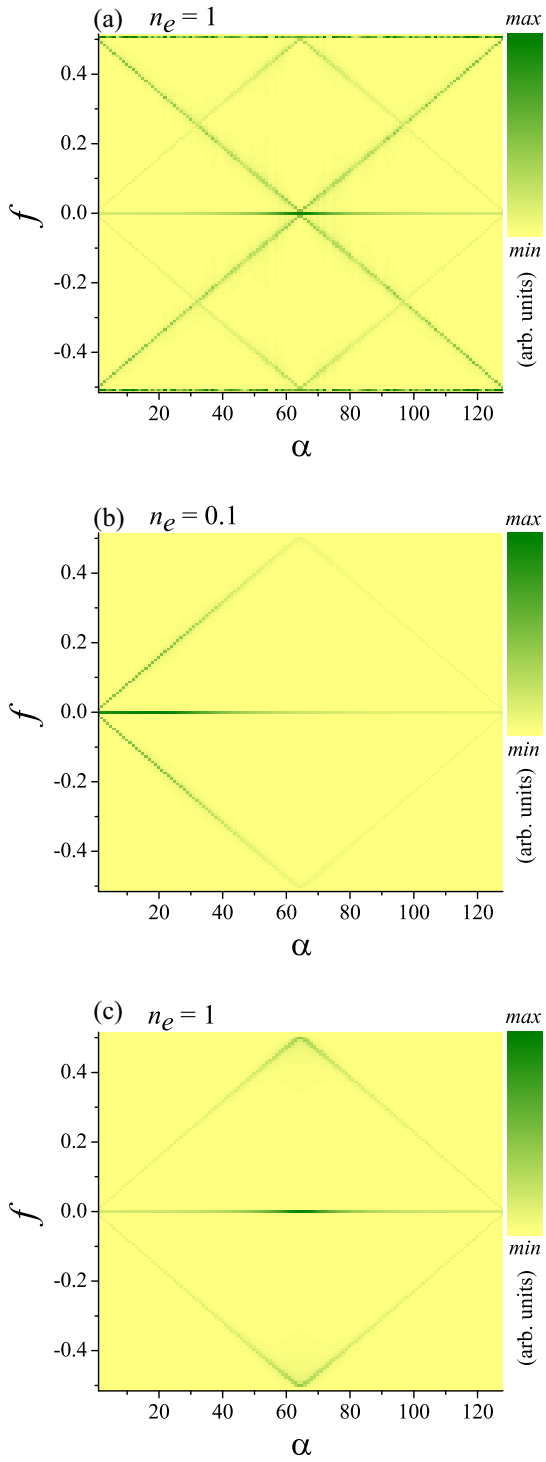

FIG. 8. Contour plot of the amplitude spectral density, $|\Delta_f^{(\alpha)}|$, shown on $f-\alpha$ plane, calculated for $n_e = 1$ [(a) and (c)] and $n_e = 0.1$ (b) to illustrate the interference in the order parameter. Calculations are performed within t-BdG [(a) and (b)] and within a-BdG [(b) and (c)].

originates from the single particle standing waves that envelope the quasiparticle $u_j^{(\alpha)}$ and quasihole $v_j^{(\alpha)}$ amplitudes at small α, as seen from Fig. 4. In the $f-\alpha$ plane, it is responsible for the line parallel to the diagonal of the plot and starting from $f = 0$ at $\alpha = 0$. This peak leads to a destructive interference in the sample body (the corresponding eigenmodes in the middle of the sample has different phases, which leads to the suppression of the oscillations) and to a constructive interference at the sample edges, reflected in the appearance of the pronounced Friedel-like oscillations in the proximity to the sample edges. We find that the amplitude of this frequency component increases with increasing α towards the middle of the band and then decreases when α approaches the band edges. The peak associated with the third frequency component is determined by $f_3(\alpha) = [f_c - \frac{2f_c}{N}\alpha]\theta(\frac{N}{2}-\alpha) + \frac{f_c}{N}(2\alpha - N)\theta(\alpha - \frac{N}{2})$. In the $f-\alpha$ plane it is given by the diagonal. Finally, the fourth peak, with the position determined by $f_4(\alpha) \approx f_c$, is the "high-frequency" component. The latter and the former components result from the high frequency pattern superimposed on the top of the single particle standing wave, seen in Fig. 4. Thus, due to the coupling between different single particle modes, which occurs in the BdG equations, the quasiparticle amplitudes $u_j^{(\alpha)}$ and the quasihole amplitudes $v_j^{(\alpha)}$ become "dressed" with the high frequency pattern. Both frequency components, $f_3(\alpha)$ and $f_4(\alpha)$, generate additional constructive interference at the edges. Indeed, when we consider the system with $n_e = 0.1$ both peaks disappear, as one may see in Fig. 8(b), which leads to a significant decrease of constructive effect of the interference at the edges (see Fig. 3).

Thus, our investigation reveals that all the self-consistent BdG eigenstates are delocalized and occupy the entire volume of the sample. The localization of the gap function in the vicinity of the surface, i.e., the surface induced enhancement of the superconductivity, is thus related to the quantum interference.

C. Anderson approximation

It is long conjectured that the Anderson approximation (a-BdG) captures all essential superconducting properties in many physically relevant situations in the presence of the time reversal symmetry [28]. Here we test this assumption with respect to the surface superconductivity by calculating the gap function for the same model and with the same microscopic parameters as above. However and most importantly, the present study brings to the light the underlying process by which the surface critical temperature becomes larger than that in the bulk.

The results for the excitation spectrum calculated by means of the a-BdG at the zero temperature are given in Fig. 9 and demonstrate a very good agreement with the spectrum obtained within the t-BdG for both $n_e = 1$ and 0.1. However, the corresponding site-profile of the order parameter have visible deviations from the t-BdG calculations and, moreover, such deviations are enhanced with increasing the temperature. Indeed, Fig. 10 displays Δ_j calculated within the a -BdG for different selected temperatures at $n_e = 1$. One sees that Δ_j has a peak at $j = 1$ for all the temperatures, with several Friedel-like oscillations ensuing towards the center of the sample. The height of the peak is smaller than that obtained in the t-BdG model. For example, at $T = 0.25$ we have $\Delta_{\text{peak}}^{(a-\text{BdG})} = 0.48$ versus $\Delta_{\text{peak}}^{(t-\text{BdG})} = 0.54$ with the difference

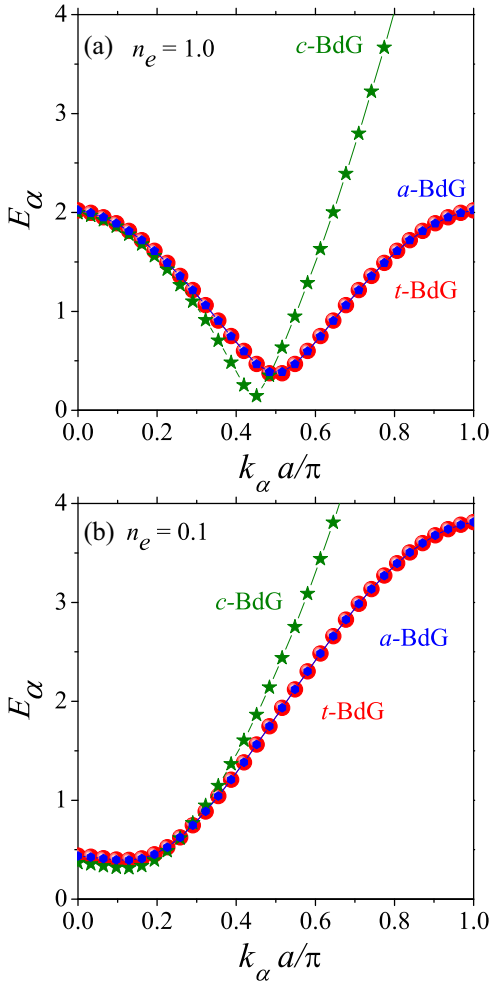

FIG. 9. Excitation spectrum E_α as a function of the quasimomentum k_α, calculated at the zero temperature within t-BdG (circles), a-BdG (rhombus) and c-BdG (stars). The calculations are done for $n_e = 1$ (a) and $n_e = 0.1$ (b), the other microscopic parameters are the same as in the previous figure.

of about 10%, while at $T = 0.16$, we obtain $\Delta_{\text{peak}}^{(a-\text{BdG})} = 0.28$ versus $\Delta_{\text{peak}}^{(t-\text{BdG})} = 0.48$ with the difference of about 40%. Thus, although the a-BdG method reproduces the Friedel-like oscillations, it significantly underestimates the amplitude of such oscillations, in agreement with the previous study of Ref. [28].

Another important difference with the full BdG calculations is that the a -BdG order parameter does not exhibit, at higher temperatures, the slow relaxation towards the center of the sample at $n_e = 1$. One sees that the corresponding Δ_j rapidly approaches Δ_B already at $j \gtrsim 10$ (Fig. 10). As a results, the surface superconductivity is not reproduced within the a-BdG approximation.

For a more detailed look, Fig. 11 displays the cumulative order parameter $\Delta_j^{(E)}$ calculated at zero temperature within the a -BdG for $n_e = 1$ (a) and 0.1 (b) (the other model parameters are the same as in Fig. 10). Here again, as in the case of t-BdG model, one observes that epigenous with similar phases close to the surface give rise to a notable enhancement of the order parameter near the edge, i.e., at $j = 1$ at $n_e = 1$ and at

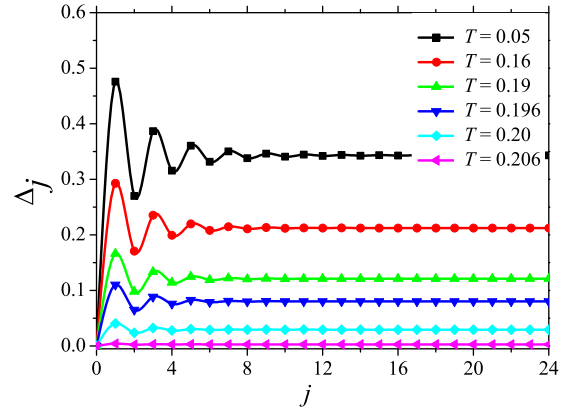

FIG. 10. Δ_j versus j, as obtained with the Anderson approximation for different selected temperatures at $n_e = 1$. Other parameters are taken the same as in Fig. 2(a).

$j = 2$ at $n_e = 0.1$. The Friedel-like oscillations are generated by the coherent summation of the partial contributions, and this is observed in both t-BdG model and a-BdG one. However, the a-BdG approximation underestimates the "coherent" peak near the boundary. Interestingly, this underestimation is more significant for the half-filling case but strongly reduces and almost disappears at $n_e = 0.1$, compare Fig. 7(b) with Fig. 11(b).

To understand the obtained underestimates of the "coherent" peak near the boundary within the a-BdG model we perform the spectral decomposition of $\Delta_j^{(\alpha)}$. Fig. 8(c) shows the amplitude spectra of $\Delta_j^{(\alpha)}$ as a contour plot in the $f - \alpha$ plane, calculated for $n_e = 1$. One can clearly observe that in case of the a-BdG model all partial contributions to the order parameter oscillate with only two dominant frequencies, $f_1(\alpha)$ and $f_2(\alpha)$. These peaks lead to a constructive interference at the sample edges, reflected in the appearance of the Friedel oscillations in the proximity of the sample edges, as one may see in Fig. 10. The first two frequency components result from an eigenoscillation of the single particle occupations, reflecting only the "bare" particlelike and holelike states, which suffices to distinctively describe bulk superconductivity. However, these components unable to cause the surface effect on the critical superconducting temperature. In the case of the system with $n_e = 0.1$ there is almost no difference in

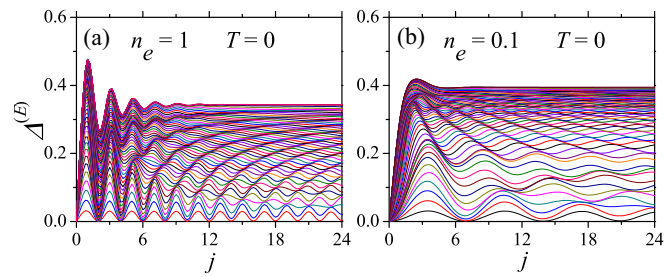

FIG. 11. The zero-temperature cumulative order parameter $\Delta_j^{(E)}$ versus j, plotted for different ascending values of $0 < E < \hbar\omega_D$ in the same manner as in Fig. 7. (a) is for $n_e = 1$ (a) and (b) corresponds to $n_e = 0.1$, the other microscopic parameters are the same as in the previous figure. Obtained within the a-BdG approximation.

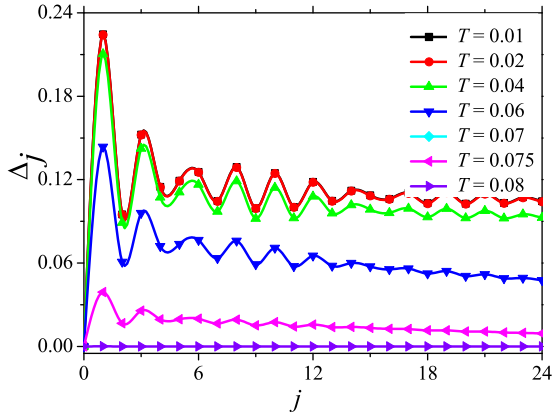

FIG. 12. Spatial profile of the order parameter Δ_j, calculated within the c-BdG model for different temperatures at $n_e = 1$ (the other model parameters are the same as in Fig. 2(a).

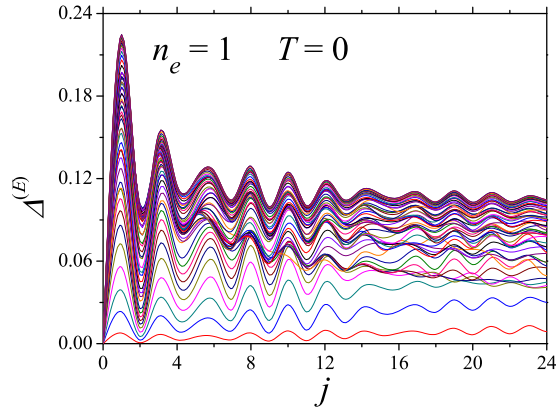

FIG. 13. The cumulative order parameter $\Delta_j^{(E)}$ for different ascending values of $0 < E < \hbar\omega_D$ (in the manner of Fig. 7). Obtained within the zero-temperature c-BdG for $n_e = 1$, the other model parameters are the same as in the previous figure.

the results obtained within t-BdG and a -BdG models. Therefore one observes no surface superconductivity in the system with $n_e = 0.1$.

Thus, irrespective of the system parameters, the a-BdG model fails to capture any increase in the critical temperature due to the surface (boundary) effects. This alters the previous conclusion of Ref. [28] that the Anderson approximation for the Bogoliubov-de Gennes formalism works well for surfaces. We find that the a-BdG model works well for surfaces only when n_e is close to zero or when it is near 2.

D. Continuous model

Here we investigate the surface induced enhancement of the critical temperature in the continuous BdG model with the quadratic dispersion of its single-particle states. The continuous model analysis allows to gain an insight into the negligible boundary effect on the critical superconducting temperature observed in Refs. [23,24] The excitation spectrum of the model, calculated for $n_e = 1$, is shown in Fig. 9 and reproduces a familiar result for a bulk superconductor.

The spatial profile of the order parameter for the continuous model is shown in Fig. 12, where $n_e = 1$ whereas the other model parameters are the same as in Figs. 2 and 10. First of all, we note that there is a general diminishing of the order parameter as compared to the previously considered BdG models. The reason is that the related DOS in the proximity to μ (the Fermi level) is considerably decreased in case of the c-BdG approach, as one can infer from Fig. 9.

In contrast to the result of the a-BdG model, the gap function profile in Fig. 12 demonstrates not only the Friedel-like oscillations in the vicinity of the surface but also the subsequent slow relaxation deep in the sample at higher temperatures. One can thus expect an enhancement of the surface superconductivity. However, the magnitude of this enhancement is vanishingly small and the effect is practically unnoticeable. This result agrees with the earlier calculations for the continuous model [23,24], discussed in the Introduction.

In addition, we calculate the cumulative order parameter $\Delta_j^{(E)}$, which is given in Fig. 13. One can see from the figure that the qualitative character of the obtained oscillations is closer to the results for t-BdG model (as compared to those for the a-BdG approach). However, the number of the contributing BdG states is significantly smaller. The absence of the states that are in coherence with those of small α is the reason for the unnoticeable surface superconducting effect.

E. Influence of surface roughness

Surface roughness can play a significant role in defining physical properties of a superconductor and, in particular, the surface related effects. For example, as it is mentioned in Introduction, it was shown that disordered (diffusive) boundaries suppress the third critical magnetic field [22] and that the ratio H_{c3}/H_{c2} becomes a nonmonotonic function of the temperature [16] and the disorder strength [21] in disordered two-band systems. Since in this work we show that the surface superconductivity is induced by the quantum interference of the contributing BdG states one could expect that such a subtle effect is suppressed by surface disorder. To check how surface disorder influences the surface critical temperature we consider isolated impurities at the surface so that $U_1 = \lambda$ and $U_N = \pm\lambda$, while all the other U_j are zero ($\lambda > 0$ is in units of t). This approach models the surface roughness. The case of $U_N = -\lambda$ produces nearly the same results as the choice $U_N = \lambda$. Thus, below we consider $U_1 = U_N = \lambda$.

Results of our calculations are summarized in Fig. 14(a), which plots the ratio T_{cS}/T_{cB} as a function of the disorder strength λ. In the calculations we assume $n_e = 1$, at which the surface superconductivity is most enhanced, and also consider four values of the coupling constant $g = 1.5$, 2, 2.5, and 3. The other microscopic parameters are the same as in Fig. 1. As expected, T_{cS}/T_{cB} is a decreasing function of λ so that the rising surface disorder tends to suppress the surface effects on the critical temperature. This conclusion holds for all considered values of the coupling constant. Moreover, our additional calculations demonstrate that the results are qualitatively independent of the cutoff parameter $\hbar\omega_D$. The enhancement of the critical temperature persists at rather moderate surface disorder with $\lambda \ll t$ and is totally suppressed by the strong disorder with $\lambda \sim t$. As one could expect, the ratio T_{cS}/T_{cB} decreases stronger in the case of the

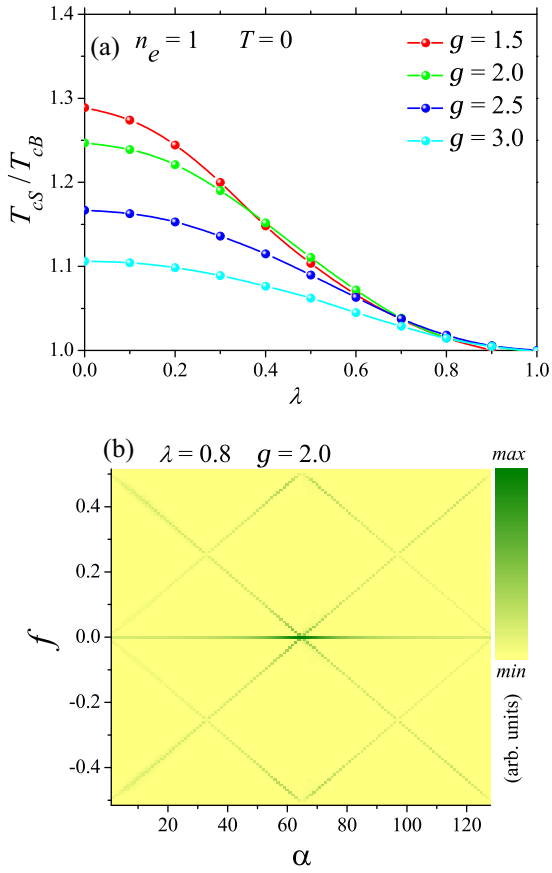

FIG. 14. (a) The ratio T_{cS}/T_{cB} as a function of the disorder strength λ, as calculated for the model with the surface disorder at different values of coupling constant. (b) Contour plot of the amplitude spectral density, $|\Delta_f^{(\alpha)}|$, shown on $f - \alpha$ plane, calculated for $n_e = 1$ and the disorder strength $\lambda = 0.8$. Calculations are performed within t-BdG.

weak coupling g. However in all considered cases, the effect holds up to the surface disorder with $\lambda \sim 0.8$–1.

Figure 14(b) illustrates the amplitude spectra of $\Delta_j^{(\alpha)}$ given by a contour plot in the $f - \alpha$ plane, calculated for $n_e = 1$, $g = 2$, and $\lambda = 0.8$. One can see that at this strength of surface disorder the third frequency component $f_3(\alpha)$ is strongly decreased as compared with that calculated for the clean sample. Furthermore, the "high-frequency" component $f_4(\alpha)$ is totally suppressed. This component of the spectrum is especially fragile with respect to surface roughness. As we showed in the previous sections, the contribution of exactly these peaks give rise to the enhancement of the critical temperature at the surface.

IV. CONCLUSIONS

This work investigates the surface superconductivity and its influence on the system critical temperature. The analysis is done by solving the three variants of the BdG equations for a one-dimensional finite chain of atoms.

Results of the tight-binding BdG model show that the order parameter can indeed be enhanced considerably in the vicinity of the surface and the surface superconductivity survives even above the bulk critical temperature. However, our study reveals that this enhancement is pronounced when the Fermi level (the chemical potential) is located in the proximity to the center of the band. When it deviates significantly from the center, the enhancement weakens and finally disappears at the band edges. Our results demonstrate that all the self-consistent BdG eigenstates are delocalized and occupy the entire volume of the sample. The localization of the gap function in the vicinity of the surface, or the surface induced enhancement of the superconductivity, is related to the quantum constructive interference between different BdG eigenstates.

Our analysis of the continuous BdG model demonstrates that although the surface effect is present in this approach, it is not pronounced. The critical temperature enhancement is almost negligible. The reason for this is a significantly lower DOS (as compared to the tight-binding equations) so that the constructive interference produces a very minor effect.

The study of the very useful Anderson approximation for the BdG equations demonstrates that this approach fails to capture the surface effect on the critical temperature. Although this approximation accurately describes the excitation spectrum, it does not reproduce correctly the dressed BdG eigenmodes in the vicinity of the surface. This gives the significant correction to the previous expectations that the Anderson approximation for the BdG formalism works well for surfaces.

Finally, our consideration of the surface disordered tight-binding BdG model reveals that the surface superconductivity enhancement is quite fragile against the surface roughness. This is contrary to the bulk disorder governed by the well-known Anderson theorem.

In summary, our quantitative findings bring out hitherto unknown features of the surface superconductivity, which, otherwise, would have remained overlooked, if we confined ourselves to only one variant of the BdG model.

We believe the theory presented here is just the tip of the iceberg of possibilities for researching surfaces superconducting effects. We hope our work motivates further efforts in the investigation of surface phenomena in superconducting systems.

ACKNOWLEDGMENTS

M.D.C acknowledges the support by the UFPE Propesq program (grant Edital Professor Visitante - Edital Propesq No. 05.2018). A.V. acknowledges hospitality and financial support from the superconductivity physics group of J. Albino Aguiar at the UFPE. Y.C. acknowledges the support by Zhejiang Provincial Natural Science Foundation (Grant No. LY18A040002). This work was supported by the Brazilian agencies, Conselho Nacional de Desenvolvimento Científico e Tecnológico CNPq (Grants No. 309374/2016-2 and No. 424304/2018-0), and Fundação de Amparo á Ciência e Tecnologia do Estado de Pernambuco FACEPE (Grant No. APQ-0936-1.05/15).

APPENDIX: MATRIX COUPLING ELEMENTS FOR *a*-BdG

In the discrete case, the interaction matrix elements are as follows:

$$g_{a\beta} = \left(\frac{2}{N+1}\right)^2 \sum_{j=0}^{N} \sin^2\left(\frac{j\alpha\pi}{N+1}\right) \sin^2\left(\frac{j\beta\pi}{N+1}\right). \quad \text{(A1)}$$

The summation results in

$$g_{a=\beta} = \frac{3}{2(N+1)} \quad \text{(A2)}$$

and

$$g_{a\neq\beta} = \frac{g^{(I)}_{a\neq\beta} + g^{(II)}_{a\neq\beta} + g^{(III)}_{a\neq\beta}}{4(N+1)^2\left[\cos\left(\frac{2\pi\alpha}{N+1}\right) - \cos\left(\frac{2\pi\beta}{N+1}\right)\right]} \quad \text{(A3)}$$

with

$$\begin{aligned} g^{(I)}_{a\neq\beta} &= 2(3+2N)\left[\cos\left(\frac{2\pi\alpha}{N+1}\right) - \cos\left(\frac{2\pi\beta}{N+1}\right)\right], \\ g^{(II)}_{a\neq\beta} &= \cos\left[2\pi\left(\alpha + \frac{N\beta}{N+1}\right)\right] - \cos\left[2\pi\left(\beta + \frac{N\alpha}{N+1}\right)\right], \\ g^{(III)}_{a\neq\beta} &= \cos\left[2\pi\left(\alpha - \frac{N\beta}{N+1}\right)\right] - \cos\left[2\pi\left(\frac{N\alpha}{N+1}\right)\right]. \end{aligned} \quad \text{(A4)}$$

This expression may be simplified as follows. Since α and β are integers then

$$\cos\left[2\pi\left(\alpha + \frac{N\beta}{N+1}\right)\right] = \cos\left[2\pi\left(\frac{N\beta}{N+1}\right)\right] \quad \text{(A5)}$$

so that

$$g^{(II)}_{a\neq\beta} + g^{(III)}_{a\neq\beta} = 2\cos\left[2\pi\frac{N\beta}{N+1}\right] - 2\cos\left[2\pi\frac{N\alpha}{N+1}\right] \quad \text{(A6)}$$

and

$$g_{a\neq\beta} = \frac{1}{2(N+1)^2}\left[3 + 2N - \frac{\sin\frac{\pi N(\alpha-\beta)}{N+1}}{\sin\frac{\pi(\alpha-\beta)}{N+1}} \frac{\sin\frac{\pi N(\alpha+\beta)}{N+1}}{\sin\frac{\pi(\alpha+\beta)}{N+1}}\right]. \quad \text{(A7)}$$

Making use of the identity

$$\sin(Nx) = \sin(x) U_{N-1}[\cos(x)], \quad \text{(A8)}$$

where

$$U_N[x] = 2^N \prod_{k=1}^{N}\left[x - \cos\frac{k\pi}{N+1}\right], \quad \text{(A9)}$$

we obtain

$$\begin{aligned} g_{a\neq\beta} = \frac{1}{2(N+1)^2}\Bigg\{3 + 2N - U_{N-1}\left[\cos\left(\frac{\pi N(\alpha-\beta)}{N+1}\right)\right] \\ \times U_{N-1}\left[\cos\left(\frac{\pi N(\alpha+\beta)}{N+1}\right)\right]\Bigg\}. \end{aligned} \quad \text{(A10)}$$

This expression is used while performing the investigation of the surface effects within the *a*-BdG model.

[1] D. Saint-James and P. G. de Gennes, Onset of superconductivity in decreasing fields, Phys. Lett. **7**, 306 (1963).

[2] D. Saint-James, Angular dependence of the upper critical field of type II superconductors, Phys. Lett. **16**, 218 (1965).

[3] D. Saint-James, E. J. Thomas, and G. Sarma, *Type-II Superconductivity* (Pergamon Press, Oxford, New York, 1969).

[4] A. A. Abrikosov, K voprosu o poverkhnostnoi sverkhprovodimosti v sil'nykh magnitnykh polyakh, J. Exptl. Theoret. Phys. (USSR) **47**, 720 (1964) [Concerning surface superconductivity in strong magnetic fields, Sov. Phys. JETP **20**, 480 (1965)].

[5] I. O. Kulik, O kriticheskom pole poverhnostnoj sverhprovodimosti i strukture sverhprovodjashhego poverhnostnogo sloja v naklonnom pole, J. Exptl. Theoret. Phys. (USSR) **55**, 889 (1969) [Critical field of surface superconductivity and the structure of a superconducting layer in an inclined fields, Sov. Phys. JETP **28**, 461 (1969)].

[6] C.-R. Hu and V. Korenman, *Critical-Field Ratio H_{c3}/H_{c2} for Pure Superconductors Outside the Landau-Ginzburg Region. I. $T \simeq 0$°K*, Phys. Rev. **178**, 684 (1969); Critical-Field RatioH_{c3}/H_{c2} for Pure Superconductors Outside the Landau-Ginzburg Region. II. $T \simeq T_c$, **185**, 672 (1969).

[7] P. Scotto and W. Pesch, On the Theory of Critical Fields of Superconducting Films, J. Low Temp. Phys. **84**, 301 (1992).

[8] C. Ebner, Temperature dependence of H_{c3}/H_{c2} in pure type-II Superconductors, Solid State Commun. **7**, 1207 (1969).

[9] A. F. Andreev, Jekzoticheskaja sverhprovodimost' ploskostej dvojnikovanija, Pis'ma Zh. Eksp. Teor. Fiz. **46**, 463 (1987) [Exotic Superconductivity of the twinning planes, JETP Lett. **46**, 584 (1989)].

[10] A. A. Abrikosov and A. I. Buzdin, Proyavlenie sverkhprovodimosti ploskostei dvoinikovaniya v vysokotemperaturnykh sverkhprovodnikakh, Pis'ma Zh. Eksp. Teor. Fiz. **47**, 204 (1988) [Manifistation of superconductivity of the twinning planes of high temperature superconductors, JETP Lett. **47**, 247 (1988)].

[11] I. N. Khlyustikov and A. I. Buzdin, Twinning-plane superconductivity, Adv. Phys. **36**, 271 (1987).

[12] N. Keller, J. L. Tholence, A. Huxley, and J. Flouque, Angular Dependence of the Upper Critical Field of the Heavy Fermion Superconductor UPt_3, Phys. Rev. Lett. **73**, 2364 (1994).

[13] V. G. Kogan, J. R. Clem, J. M. Deang, and M. D. Gunzburger, Nucleation of superconductivity in finite anisotropic superconductors and the evolution of surface superconductivity toward the bulk mixed state, Phys. Rev. B **65**, 094514 (2002).

[14] K. V. Samokhin, Poverhnostnoe kriticheskoe pole v sverhprovodnikah s anizotropnym sparivaniem, J. Exptl. Theoret. Phys. **107**, 906 (1995) [Surface critical field in superconductors

with anisotropic pairing, JETP **80**, 515 (1995)]; Surface Critical Field in Unconventional Superconductors, Europhys. Lett. **32**, 675 (1995).

[15] A. Rydh, U. Welp, J. M. Hiller, A. E. Koshelev, W. K. Kwok, G. W. Crabtree, K. H. P. Kim, K. H. Kim, C. U. Jung, H.-S. Lee, B. Kang, and S.-I. Lee, Surface contribution to the superconducting properties of MgB_2 single crystals, Phys. Rev. B **68**, 172502 (2003).

[16] D. A. Gorokhov, Surface Superconductivity of Dirty Two-Band Superconductors: Applications to MgB_2, Phys. Rev. Lett. **94**, 077004 (2005).

[17] D.-J. Jang, H.-S. Lee, B. Kang, H.-G. Lee, M.-H. Cho, and S.-I. Lee, Two-band effect on the temperature and the angle dependences of the ratio of the surface to the bulk superconductivity in MgB_2, New J. Phys. **11**, 073028 (2009).

[18] V. V. Moshchalkov, L. Gielen, C. Strunk, R. Jonckheere, X. Qiu, C. Van Haesendonck, and Y. Bruynseraede, Effect of sample topology on the critical fields of mesoscopic superconductors, Nature **373**, 319 (1995).

[19] V. A. Schweigert and F. M. Peeters, Influence of the confinement geometry on surface superconductivity, Phys. Rev. B **60**, 3084 (1999).

[20] I. L. Aleiner, A. V. Andreev, and V. Vinokur, Aharonov-Bohm Oscillations in Singly Connected Disordered Conductors, Phys. Rev. Lett. **114**, 076802 (2015).

[21] H.-Y. Xie, V. G. Kogan, M. Khodas, and A. Levchenko, Onset of surface superconductivity beyond the Saint-James–de Gennes limit, Phys. Rev. B **96**, 104516 (2017).

[22] D. F. Agterberg and M. B. Walker, Effect of diffusive boundaries on surface superconductivity in unconventional superconductors, Phys. Rev. B **53**, 15201 (1996).

[23] T. Giamarchi and M. T. Beal-Monod, O. T. Valls, Onset of surface superconductivity, Phys. Rev. B **41**, 11033 (1990).

[24] B. P. Stojkovic, O. T. Valls, Order parameter near a superconductor-insulator interface, Phys. Rev. B **47**, 5922 (1993).

[25] R. J. Troy and A. T. Dorsey, Self-consistent microscopic theory of surface superconductivity, Phys. Rev. B **51**, 11728 (1995).

[26] A. M. Martin, J. F. Annett, Self-consistent interface properties of d- and s-wave superconductors, Phys. Rev. B **57**, 8709 (1997).

[27] A. Samoilenka and E. Babaev, Boundary states with elevated critical temperatures in Bardeen-Cooper-Schrieffer superconductors, Phys. Rev. B **101**, 134512 (2020).

[28] K. Tanaka and F. Marsiglio, Anderson prescription for surfaces and impuritie, Phys. Rev. B **62**, 5345 (2000).

[29] P. G. de Gennes, *Superconductivity of Metals and Alloys* (W. A. Benjamin, New York, 1966).

[30] A. V. Swidzinsky, *Spatially Inhomogeneous Problems in the Theory of Superconductivity* (Nauka, Moscow, 1982).

[31] A. Cichy and A. Ptok, Superfluidity of fermionic pairs in a harmonic trap. Comparative studies: Local Density Approximation and Bogoliubov-de Gennes solutions, J. Phys. Commun. **4**, 055006 (2020).

[32] A. A. Shanenko and M. D. Croitoru, Shape resonances in the superconducting order parameter of ultrathin nanowires, Phys. Rev. B **73**, 012510 (2006).

[33] M. D. Croitoru, A. A. Shanenko, and F. M. Peeters, Metallic nanograins: Spatially nonuniform pairing induced by quantum confinement, Phys. Rev. B **83**, 214509 (2007).

[34] J.-X. Zhu, *Bogoliubov-de Gennes Method and Its Applications*, Lecture Notes in Physics Book Vol. 924 (Springer International Publishing, Switzerland, 2016).

[35] T. X. R. Souza and F. Marsiglio, Systematic study of the superconducting critical temperature in two- and three-dimensional tight-binding models: A possible scenario for superconducting H_3S, Phys. Rev. B **94**, 184509 (2016).

[36] A. Shanenko, M. D. Croitoru, and F. M. Peeters, Superconducting nanofilms: Andreev-type states induced by quantum confinement, Phys. Rev. B **78**, 054505 (2008).

[37] M. D. Croitoru, A. A. Shanenko, C. C. Kaun, and F. M. Peeters, Superconducting nanowires: Interplay of discrete transverse modes with supercurrent, Phys. Rev. B **80**, 024513 (2009).

[38] M. M. Doria, M. Cariglia, and A. Perali, Multigap superconductivity and barrier-driven resonances in superconducting nanofilms with an inner potential barrier, Phys. Rev. B **94**, 224513 (2016).

[39] M. D. Croitoru, A. A. Shanenko, F. M. Peeters, and V. M. Axt, Parity-fluctuation induced enlargement of the ratio $\Delta E/k_B T_c$ in metallic grains, Phys. Rev. B **84**, 214518 (2011).